

Low-energy ${}^3\text{He}(\alpha,\alpha){}^3\text{He}$ elastic scattering and the ${}^3\text{He}(\alpha,\gamma){}^7\text{Be}$ reaction

Peter Mohr*

Diakonie-Klinikum Schwäbisch Hall, D-74523 Schwäbisch Hall, Germany

(Dated: November 11, 2018)

The cross sections of the ${}^3\text{He}(\alpha,\alpha){}^3\text{He}$ and ${}^3\text{He}(\alpha,\gamma){}^7\text{Be}$ reactions are studied at low energies using a simple two-body model in combination with a double-folding potential. At very low energies the capture cross section is dominated by direct s -wave capture. However, at energies of several MeV the d -wave contribution increases, and the theoretical capture cross section depends sensitively on the strength of the $L = 2$ potential. Whereas the description of the $L = 2$ elastic phase shift requires a relatively weak potential strength, recently measured capture data can only be described with a significantly enhanced $L = 2$ potential. A simultaneous description of the new experimental capture data and the elastic phase shifts is not possible within this model. Because of the dominating extranuclear capture, this conclusion holds in general for most theoretical models.

PACS numbers: 25.55.-e, 25.55.Ci, 24.50.+g, 25.40.Lw

I. INTRODUCTION

The ${}^3\text{He}(\alpha,\gamma){}^7\text{Be}$ capture reaction is a key reaction in nuclear astrophysics. The flux of solar neutrinos at higher energies depends on the branching between the ${}^3\text{He}({}^3\text{He},2p)\alpha$ and ${}^3\text{He}(\alpha,\gamma){}^7\text{Be}$ reactions, and in big-bang nucleosynthesis ${}^7\text{Li}$ can be produced via the ${}^3\text{He}(\alpha,\gamma){}^7\text{Be}$ capture reaction and subsequent electron capture of ${}^7\text{Be}$ [1]. While the energy range of big-bang nucleosynthesis is covered by experimental data, the experiments are approaching the Gamow window around $E_0 = 22\text{ keV}$ of the ${}^3\text{He}(\alpha,\gamma){}^7\text{Be}$ reaction in the sun, but still have not reached E_0 .

Very recently, it has been attempted successfully to extend the measured energy range of the ${}^3\text{He}(\alpha,\gamma){}^7\text{Be}$ reaction to higher energies up to about 3.2 MeV [2]. From these new experimental data the energy dependence of the ${}^3\text{He}(\alpha,\gamma){}^7\text{Be}$ capture reaction can be extracted and compared to theoretical predictions. A better theoretical understanding of the energy dependence will help to reduce the uncertainties of the extrapolation of the cross section down to the Gamow window at the temperature of the interior of our sun. Several further experimental data sets exist at lower energies [3, 4, 5, 6, 7, 8, 9, 10, 11, 12, 13, 14, 15, 16, 17] that are summarized in two recent compilations [18, 19].

Besides theoretical calculations shown in the experimental papers [3, 4, 5, 6, 7, 8, 9, 10, 11, 12, 13, 14, 15, 16, 17], various theoretical studies have been devoted to the analysis of the ${}^3\text{He}(\alpha,\gamma){}^7\text{Be}$ capture cross section [20, 21, 22, 23, 24, 25, 26, 27, 28, 29, 30, 31, 32, 33, 34, 35, 36, 37, 38, 39]. Additionally, a review on the status of the ${}^3\text{He}(\alpha,\gamma){}^7\text{Be}$ reaction is given in [40].

Theoretical models can be significantly constrained by the request that elastic scattering data have to be described simultaneously with the capture data. Phase shifts have been derived from elastic scattering angular

distributions in [41, 42, 43], and angular distributions or excitation functions at low energies are reported in [31, 44, 45, 46].

It will be shown that the capture cross section of the ${}^3\text{He}(\alpha,\gamma){}^7\text{Be}$ reaction at low energies is dominated by E1 transitions from incoming s - and d -waves to bound p -states in ${}^7\text{Be}$. Consequently, a precise description of the s -wave and d -wave phase shifts is a prerequisite for the calculation of the ${}^3\text{He}(\alpha,\gamma){}^7\text{Be}$ capture cross section.

This article is organized as follows. In Sec. II a brief description of the direct capture model is provided. General remarks on the applicability and reliability of this model and other theoretical calculations are given in Sec. III. Results for the ${}^3\text{He}(\alpha,\alpha){}^3\text{He}$ elastic scattering and ${}^3\text{He}(\alpha,\gamma){}^7\text{Be}$ capture cross sections are presented in Sec. IV, and theoretical uncertainties are carefully analyzed. Conclusions are drawn in Sec. V, and finally a brief summary is given in Sec. VI.

All energies E are given in the center-of-mass system throughout this paper except explicitly noted. Excitation energies E^* in ${}^7\text{Be}$ are related to E by $E^* = E + Q$ with the Q -value of the ${}^3\text{He}(\alpha,\gamma){}^7\text{Be}$ reaction $Q = 1586.6\text{ keV}$ [47].

II. THE DIRECT CAPTURE MODEL

The direct capture (DC) model is a simple but powerful model to calculate capture cross sections between light nuclei. The full formalism is given explicitly in [48], and its application together with systematic folding potentials is described in detail in our previous work on the ${}^3\text{He}(\alpha,\alpha){}^3\text{He}$ and ${}^3\text{He}(\alpha,\gamma){}^7\text{Be}$ reactions [31]. Here I only repeat some essential features of the DC model that are important for the following discussion.

The theoretical capture cross section σ_{th} is given by the product of the DC cross section σ_{DC} and the spectroscopic factor C^2S of the final state:

$$\sigma_{\text{th}} = C^2S \times \sigma_{\text{DC}} \quad (2.1)$$

The DC cross section depends on the square of the over-

*E-mail: WidmaierMohr@t-online.de

lap between the scattering wave function $\chi_{L_i, J_i}(r)$, the bound state wave function $u_{N, L_f, J_f}(r)$, and the electromagnetic operator $\mathcal{O}^{E1, E2, M1}$ of $E1$, $E2$, and $M1$ transitions:

$$\sigma_{\text{DC}} \sim \left| \int \chi_{L_i, J_i}(r) \mathcal{O}^{E1, E2, M1} u_{N, L_f, J_f}(r) dr \right|^2 \quad (2.2)$$

where L_i, J_i and L_f, J_f are the angular momenta in the initial scattering wave function $\chi(r)$ and the final bound state wave function $u(r)$. N is the number of nodes in the bound state wave function that takes into account the Wildermuth condition. The total number of oscillator quanta $Q = 2N + L_f = 3$ for three nucleons in the $1p$ shell leads to two cluster states in ${}^7\text{Be}$. There is a first state with one node ($N = 1$) and angular momentum $L = 1$, and a second state without node ($N = 0$) and $L = 3$. Both states are split into doublets because of the spin $S = 1/2$ of the ${}^3\text{He}$ nucleus. Both $L = 1$ states are located below the ${}^3\text{He}-\alpha$ threshold in ${}^7\text{Be}$, whereas the $L = 3$ states are located above the threshold and may appear as resonances in the ${}^3\text{He}(\alpha, \gamma){}^7\text{Be}$ capture reaction. Properties of the cluster states are given in Table I, and a simplified level scheme of ${}^7\text{Be}$ is shown in Fig. 1.

TABLE I: Level scheme of ${}^7\text{Be}$. Experimental data are taken from [47]. The potential strength parameters are adjusted to reproduce the energies of the bound and quasi-bound states (see text).

L	J^π	E_{exp}^* (keV)	$E_{\text{exp}} = E_{\text{calc}}$ (keV)	Γ_{exp} (keV)	Γ_{calc} (keV)
1	$3/2^-$	0	-1586.6^a ($T_{1/2} = 53.22$ d)	–	–
1	$1/2^-$	429.1 ± 0.1	-1157.5^a ($\tau = 192 \pm 25$ fs)	–	–
3	$7/2^-$	4570 ± 50	2983.4^a	175 ± 7	145
3	$5/2^-$	6730 ± 100	5143.4^a	≈ 1200	≈ 1100

^apotential adjusted

The bound state wave functions $u(r)$ are shown for the $L = 1, J^\pi = 3/2^-$ ground state and the $L = 1, J^\pi = 1/2^-$ first excited state in ${}^7\text{Be}$ in Fig. 2. Fig. 3 shows the integrand of Eq. (2.2), i.e. the overlap of the scattering wave function $\chi(r)$, the electromagnetic operator \mathcal{O} , and the bound state wave function $u(r)$ for different transitions in the ${}^3\text{He}(\alpha, \gamma){}^7\text{Be}$ capture reaction at a very low (100 keV) and at a higher energy (3 MeV). A detailed discussion will be given in the following Sec. III.

The basic ingredient for the calculation of the DC integral in Eq. (2.2) are the potentials for the entrance channel (elastic scattering) and the exit channel (bound state wave function). As soon as the potentials are fixed, the DC integral is calculated without further adjustment of parameters to experimental capture data. The spectroscopic factor C^2S of the bound state is taken – exactly as in [31] – from theory in the present study: $C^2S(3/2^-) = 1.174$ and $C^2S(1/2^-) = 1.175$ [49]. The

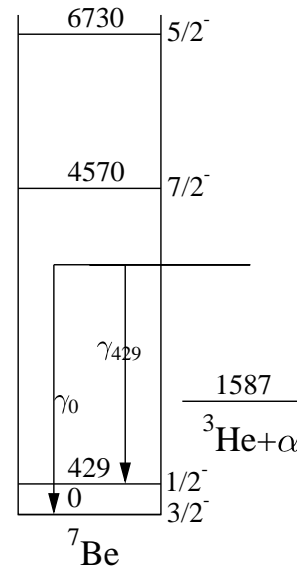


FIG. 1: Simplified level scheme of ${}^7\text{Be}$ with the $L = 1$ and $L = 3$ cluster states. Excitation energies E^* are given in keV. All data are taken from [47].

spectroscopic factor is considered as an absolute normalization for the calculated capture cross section, similar to the procedure in [50]. It is beyond the scope of the present paper to discuss the relation between the asymptotic normalization coefficient and the spectroscopic factor as e.g. in [51] because the main conclusions of this work are not affected.

The potential for the ${}^3\text{He} - \alpha$ system is the sum of the central nuclear potential, the spin-orbit potential, and the Coulomb potential. The real part of the central nuclear potential is calculated from the double folding procedure [52, 53] that is scaled by a strength parameter λ which is about 1.4 – 1.8 in this study. The underlying nuclear densities are derived from the measured charge density distributions [54]. The imaginary part of the nuclear potential can be set to zero because there are no open channels below 4 MeV except the relatively weak ${}^3\text{He}(\alpha, \gamma){}^7\text{Be}$ capture. The spin-orbit potential is taken in the usual Thomas form proportional to $1/r \times dV/dr$, again scaled by a spin-orbit strength parameter λ_{LS} . Finally, the Coulomb potential V_C is calculated from the homogeneous charged sphere model with a Coulomb radius R_C identical to the root-mean-square radius of the folding potential: $R_C = r_{\text{rms}} = 2.991$ fm. Further details can be found in [31]. The total potential is given by:

$$V(r) = \lambda V_F(r) + \lambda_{LS} \frac{\text{fm}^2}{r} \frac{dV_F(r)}{dr} \vec{L} \vec{S} + V_C(r) \quad (2.3)$$

with the unscaled ($\lambda = 1$) folding potential $V_F(r)$. The factor fm^2 in the spin-orbit potential is added to obtain a dimensionless strength parameter λ_{LS} . \vec{L} , \vec{S} , and $\vec{J} = \vec{L} + \vec{S}$ are the orbital, spin, and total angular momenta in units of \hbar .

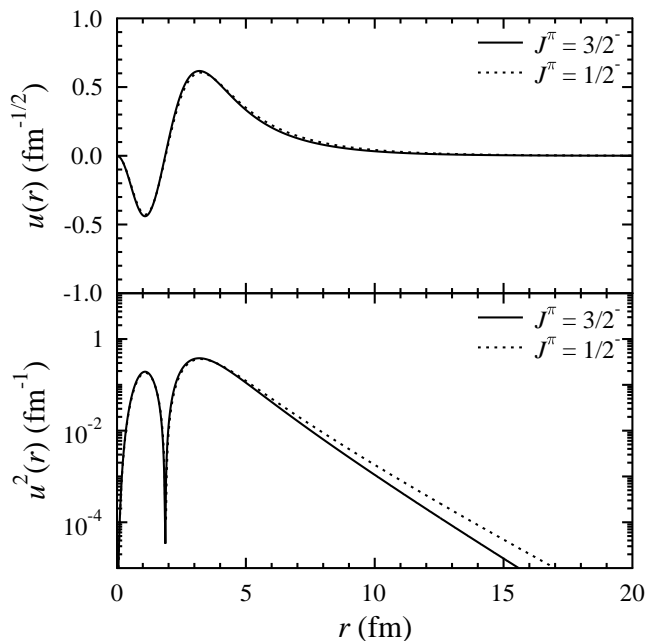


FIG. 2: Bound state wave functions $u(r)$ for the $L = 1$, $J^\pi = 3/2^-$ ground state and the $L = 1$, $J^\pi = 1/2^-$ first excited state in ${}^7\text{Be}$ in linear scale (upper) and $u^2(r)$ in logarithmic scale (lower). The wave functions are very similar in the nuclear interior. The slope in the exterior reflects the different binding energies ($E_B = -1587$ keV for the $3/2^-$ ground state and $E_B = -1158$ keV for the $1/2^-$ first excited state).

One main advantage of folding potentials is the small number of adjustable parameters. The shape of the potential is fixed by the folding procedure. Only the strength parameters λ and λ_{LS} have to be adjusted to experimental data. Obviously, the small number of adjustable parameters improves the predictive power of the calculations.

The shape of the folding potential for ${}^3\text{He} - \alpha$ is almost Gaussian. Consequently, the spin-orbit part has almost the same shape, and the sum of central and spin-orbit potential again has the same shape. In other words, the spin-orbit potential slightly increases the potential for $J = L + 1/2$ waves and slightly decreases the potential for the $J = L - 1/2$ waves but keeps the shape of the folding potential. Alternatively, the same effect can be obtained if the spin-orbit potential is set to zero and instead the strength parameter of the central potential becomes J -dependent. This approach has been followed e.g. in [32]: there very similar results to our previous work [31] were obtained using empirical Gaussian potentials with a J -dependent depth V_0 .

III. GENERAL REMARKS

The nucleus ${}^7\text{Be}$ and the ${}^3\text{He}(\alpha, \alpha){}^3\text{He}$ elastic scattering and ${}^3\text{He}(\alpha, \gamma){}^7\text{Be}$ capture reactions are textbook examples for the successful application of a simple two-body

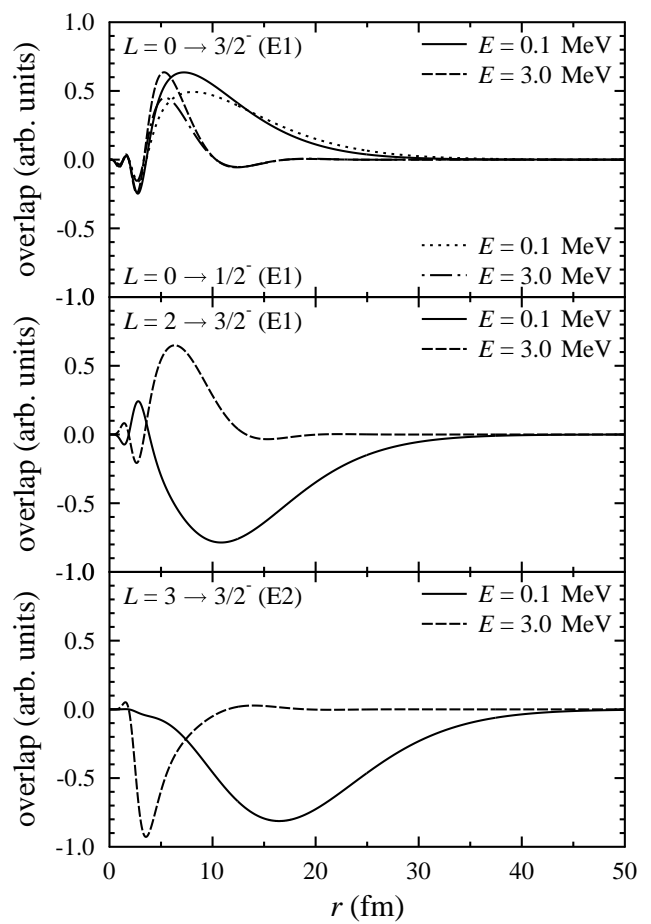


FIG. 3: Overlap of the scattering wave function $\chi(r)$, electromagnetic transition operator \mathcal{O} , and bound state wave function $u(r)$ for different transitions of the ${}^3\text{He}(\alpha, \gamma){}^7\text{Be}$ capture reaction. Upper: Non-resonant $E1$ s -wave capture to the $3/2^-$ ground state and $1/2^-$ first excited state at energies $E = 0.1$ MeV and 3.0 MeV. Middle: Non-resonant $E1$ d -wave capture to the $3/2^-$ ground state at $E = 0.1$ MeV and 3.0 MeV. Lower: Non-resonant and resonant $E2$ f -wave capture to the $3/2^-$ ground state at $E = 0.1$ MeV and 3.0 MeV. Further discussion see text.

model because of the strong internal binding energies of the two constituents ${}^3\text{He}$ and ${}^4\text{He}$. Early calculations have been performed for the ${}^3\text{He}(\alpha, \gamma){}^7\text{Be}$ reaction using hard-sphere phase shifts for the entrance channel, thus considering external capture only. Already these early calculations have successfully reproduced the cross section of the ${}^3\text{He}(\alpha, \gamma){}^7\text{Be}$ capture reaction at low energies [20, 21, 22]. Nowadays it must be the aim of theoretical studies to reproduce simultaneously the ${}^3\text{He}(\alpha, \alpha){}^3\text{He}$ elastic scattering cross sections and phase shifts, the ${}^3\text{He}(\alpha, \gamma){}^7\text{Be}$ capture reaction, and electromagnetic properties of the ${}^7\text{Be}$ nucleus. Often also the mirror nucleus ${}^7\text{Li}$ and the mirror reaction ${}^3\text{H}(\alpha, \gamma){}^7\text{Li}$ are considered. The present study focuses on the new results for the ${}^3\text{He}(\alpha, \gamma){}^7\text{Be}$ reaction [2]; the ${}^7\text{Li}$ mirror system was already studied in our earlier work [31].

Only very few radiation widths Γ_γ or lifetimes τ have been measured for the ${}^7\text{Be}$ nucleus. The first excited $1/2^-$ state in ${}^7\text{Be}$ decays by a $M1$ transition to the ${}^7\text{Be}$ ground state with a lifetime of $\tau_m = 192 \pm 25$ fs [47] corresponding to $B(M1, 3/2^- \rightarrow 1/2^-) = 1.87 \pm 0.25 \mu_N^2$. Following the formalism in [38, 55, 56], the reduced transition strength $B(M1, 3/2^- \rightarrow 1/2^-)$ is given by

$$B(M1) = \frac{1}{4\pi} [2\mu({}^3\text{He}) - \mu_N G]^2 |\langle u_{3/2^-} | u_{1/2^-} \rangle|^2 \quad (3.1)$$

with the effective cluster-cluster orbital gyromagnetic factor $G = (Z_1 A_2^2 + Z_2 A_1^2) / [A_1 A_2 (A_1 + A_2)] = 0.5952$ for ${}^7\text{Be} = {}^3\text{He} \otimes \alpha$ and $\mu({}^3\text{He}) = -2.1276 \mu_N$ [57]. As already pointed out in [30], the overlap of the bound state wave functions $|\langle u_{3/2^-} | u_{1/2^-} \rangle|^2$ is close to unity because both wave functions $u(r)$ are very similar. This similarity is also obvious for the wave functions in this study, see Fig. 2; here the overlap deviates by less than one per cent from unity. Consequently, the reduced transition strength $B(M1)$ is practically defined by the factor $\frac{1}{4\pi} [2\mu({}^3\text{He}) - \mu_N G]^2 = 1.873 \mu_N^2$ which is in excellent agreement with the experimental result of $1.87 \pm 0.25 \mu_N^2$. The excellent reproduction of the $B(M1)$ transition strength between the $3/2^-$ ground state and the $1/2^-$ first excited state in ${}^7\text{Be}$ is thus a more or less trivial result for any two-body calculation with realistic bound state wave functions.

The $E2$ contribution of this transition is orders of magnitude smaller than the $M1$ transition because of the relatively low transition energy of $E_\gamma = 429$ keV and the strong E_γ^5 dependence of $E2$ transitions: one $E2$ Weisskopf unit corresponds to a radiation width of about $\Gamma_\gamma(E2) \approx 10$ neV which has to be compared to the experimental $M1$ width of $\Gamma_\gamma = 3.4$ meV.

No further experimental data for radiation widths in ${}^7\text{Be}$ exist in [47]. However, the recent experiment [2] has measured the cross section of the ${}^3\text{He}(\alpha, \gamma){}^7\text{Be}$ reaction in the $7/2^-$ resonance for the first time, and it was possible to derive the radiation width $\Gamma_{\gamma,0}$ in [2]. It will be shown in Sec. IV B that the DC model is able to reproduce the experimental value within its relatively large experimental uncertainty. Contrary to the above studied $M1$ transition, this result is not trivial because it requires the overlap of the $7/2^-$ scattering wave function, the $E2$ operator, and the $3/2^-$ ground state wave function (see Fig. 3, lower part).

Often, “direct capture” is also named “extranuclear capture” or “non-resonant capture”. The origin of these somewhat misleading names comes from the early calculations by Christy and Duck [20] and Tombrello and coworkers [21, 22]. A good description of the experimental ${}^3\text{He}(\alpha, \gamma){}^7\text{Be}$ capture cross section was obtained in [20, 21, 22] using hard-sphere phase shifts for the non-resonant s - and d -waves (that are by definition non-resonant). As can be seen from Fig. 3 (upper and middle parts), the main contribution of the $E1$ transitions from incoming s -waves and d -waves to the bound $L = 1$

states comes indeed from the nuclear exterior, thus validating the hard-sphere approximation for the s -waves and d -waves in [20, 21, 22]. However, as can be seen from Fig. 3 (lower part), the main contribution of the $E2$ transition from the incoming f -wave to the $3/2^-$ ground state comes from the exterior at the low energy of $E = 100$ keV, but is shifted to the interior at $E = 3.0$ MeV which is in the $7/2^-$ resonance. Thus, the terminus “direct capture” is neither identical to “extranuclear capture” nor to “non-resonant capture”. This has also been illustrated for the 3^+ resonance in the ${}^2\text{H}(\alpha, \gamma){}^6\text{Li}$ reaction in [58].

IV. RESULTS

A. Elastic scattering cross sections and phase shifts

As already pointed out above, the parameters of the potential – i.e. the potential strength parameters λ and λ_{LS} – have to be adjusted to experimental data. Elastic scattering phase shifts are typically used for this adjustment. Such phase shifts have been derived from angular distributions and excitation functions over a broad range of energies [41, 42, 43], see Fig. 4.

The data of Spiger and Tombrello cover the energy range slightly below the $7/2^-$ resonance and range from about 2.5 MeV up to 10 MeV [41]. The data of Boykin *et al.* cover the energy range from about 1.9 MeV up to 4 MeV. However, no numerical results are given for the important d -waves. Instead, it is pointed out that “the values obtained at the various energies were scattered with no discernible trend in a band between -4° and $+4^\circ$ ” [42]. The data from Hardy *et al.* start above the $7/2^-$ resonance and range from about 3.3 MeV up to 7.7 MeV [43].

The adjustment of the potential strength parameters λ and λ_{LS} is done as follows. The procedure is almost identical to the previous work [31] with a modification of the spin-orbit potential. First, the strength parameter λ is adjusted to the s -wave phase shift. This can be done unambiguously because the s -wave is not affected by the spin-orbit potential. An excellent agreement with the experimental phase shifts is obtained with $\lambda(L = 0) = 1.452$ (full black line in Fig. 4, upper part). Additionally, the results are shown for a variation of the strength parameter λ between 1.4 and 1.6 (green dashed, red dotted, and blue narrow-dashed lines) that will be important for the analysis of the ${}^3\text{He}(\alpha, \gamma){}^7\text{Be}$ capture cross section in Sec. IV B.

The parameter $\lambda(L = 0) = 1.452$ is also used for the d -wave phase shifts. As can be seen from Fig. 4, there is excellent agreement with the experimental d -wave phase shifts over a broad energy range. There is no evidence for a different behavior of the $d_{3/2}$ and $d_{5/2}$ phase shifts from the data in [41, 42, 43]. Thus, the spin-orbit potential has to vanish for the d -waves, and $\lambda_{LS}(L = 2) = 0$. It is interesting to note that any deviation of the potential strength from $\lambda = 1.452$ leads to deviations of the calcu-

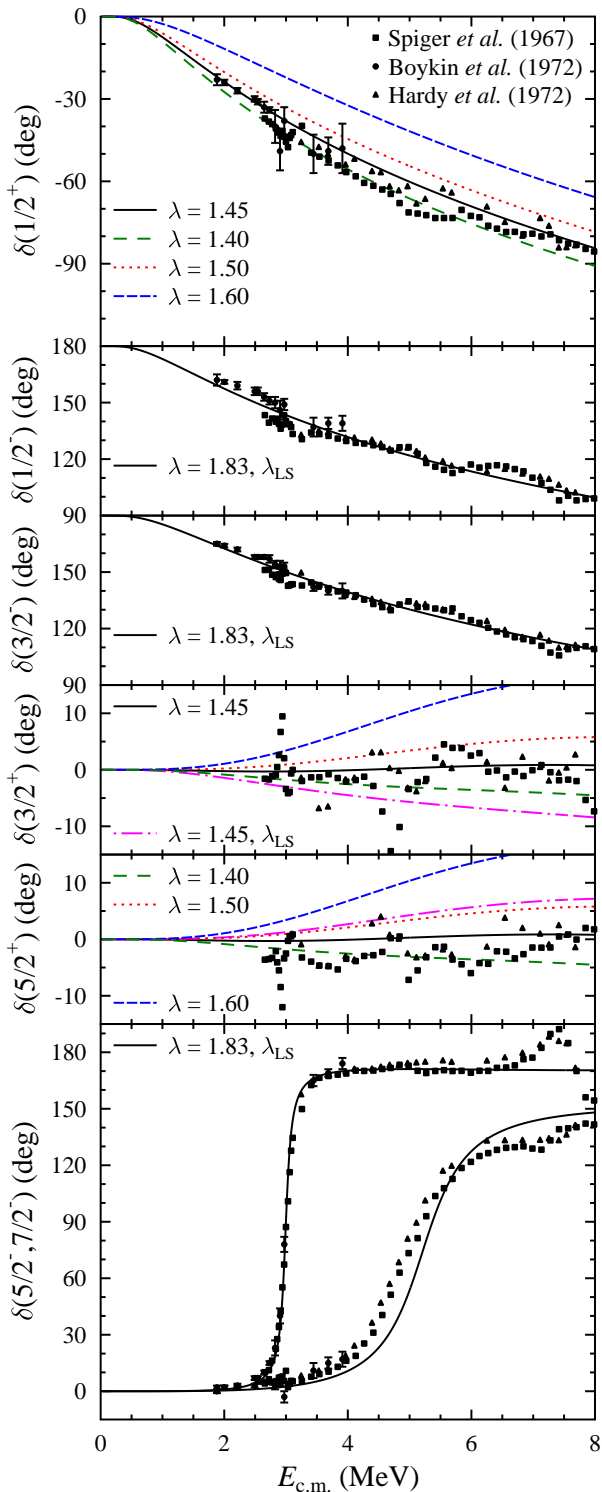


FIG. 4: (Color online) Phase shifts for elastic ${}^3\text{He}(\alpha, \alpha){}^3\text{He}$ scattering. Experimental data are taken from [41, 42, 43]. Calculations are performed using the potential strength parameters $\lambda^{\text{even}} = 1.452$, $\lambda_{LS}^{\text{even}} = 0$, $\lambda^{\text{odd}} = 1.830$ and $\lambda_{LS}^{\text{odd}} = -0.173$ (standard case, full black line). The parameter λ^{even} is varied between 1.40 and 1.60 ($\lambda^{\text{even}} = 1.40$: green dashed line; $\lambda^{\text{even}} = 1.50$: red dotted line; $\lambda^{\text{even}} = 1.60$: blue narrow-dashed line), and the spin-orbit strength of the odd partial waves has also been used for the even partial waves ($\lambda^{\text{even}} = 1.452$, $\lambda_{LS}^{\text{even}} = -0.173$: magenta dash-dotted line). Further discussion see text.

lated d -wave phase shifts from the experimentally vanishing data. Combining the results for the s -wave and the d -waves, the potential strength parameters for even partial waves are $\lambda^{\text{even}} = 1.452$ and $\lambda_{LS}^{\text{even}} = 0$. A test with the spin-orbit strength derived from the f -waves (see below) also shows clear disagreement to the experimental d -wave phase shifts (magenta dash-dotted line in Fig. 4).

A noticeably higher value for the potential strength λ is found for the odd partial waves. λ^{odd} and $\lambda_{LS}^{\text{odd}}$ have been adjusted to reproduce the energies of the f -wave resonances (see Fig. 4). This leads to $\lambda^{\text{odd}} = 1.830$ and $\lambda_{LS}^{\text{odd}} = -0.173$. Using these values, an excellent agreement for the f -wave phase shifts is obtained in both non-resonant and resonant energy regions. In particular, the resonance widths are properly reproduced (see also Table I). Good agreement with the experimental p -wave phase shifts is also obtained with the above λ^{odd} and $\lambda_{LS}^{\text{odd}}$. The parameters λ^{odd} and $\lambda_{LS}^{\text{odd}}$ were not varied in the following study because any change of these parameters shifts the f -wave resonances dramatically in energy.

The new experimental ${}^3\text{He}(\alpha, \gamma){}^7\text{Be}$ capture data cover an energy range that is at the lower end of the experimental phase shift data of [41, 42, 43]. Fortunately, further experimental angular distributions of ${}^3\text{He}(\alpha, \alpha){}^3\text{He}$ elastic scattering are available in [31, 44, 46] in the relevant energy range of the new ${}^3\text{He}(\alpha, \gamma){}^7\text{Be}$ experiment [2]. These experimental angular distributions are compared to the calculated cross sections using the above determined parameters $\lambda^{\text{even}} = 1.452$, $\lambda_{LS}^{\text{even}} = 0$, $\lambda^{\text{odd}} = 1.830$ and $\lambda_{LS}^{\text{odd}} = -0.173$. The result is shown in Fig. 5 (full black lines). Additionally, again the sensitivity on the potential strength parameters λ^{even} and $\lambda_{LS}^{\text{even}}$ is analyzed (colored dashed and dotted lines in Fig. 5).

The conclusions from Fig. 5 are clear. As expected, an excellent agreement between the experimental data and the calculations is only obtained using the same parameters as derived from the phase shifts of [41, 42, 43] in Fig. 4. From the shown angular distributions the parameter λ^{even} may vary between 1.40 and 1.45; a careful inspection of the phase shift calculations in Fig. 4 shows that the low-energy s -wave phase shifts of [42] and the overall energy dependence are best described using $\lambda^{\text{even}} = 1.45$; however, the data from [41] are better described using $\lambda^{\text{even}} = 1.40$ (green dashed line in Fig. 4). Because of the better overall description of the s -wave phase shifts and the excellent description of the d -wave phase shifts I take $\lambda^{\text{even}} = 1.45$, $\lambda_{LS}^{\text{even}} = 0$ as the standard calculation in the following, keeping $\lambda^{\text{odd}} = 1.830$ and $\lambda_{LS}^{\text{odd}} = -0.173$ fixed for the odd partial waves. An additional calculation with $\lambda^{\text{even}} = 1.45$, $\lambda_{LS}^{\text{even}} = -0.173$ (instead of $\lambda_{LS}^{\text{even}} = 0$) is almost identical to the previous calculation in [31] except minor technical modifications (e.g. larger integration range and smaller step size).

A minor disagreement between the calculated angular distribution and the experimental data can be seen at $E = 2715$ keV. This is not very surprising because this energy is at the low-energy tail of the $7/2^-$ resonance. The width of this resonance is slightly underestimated: the

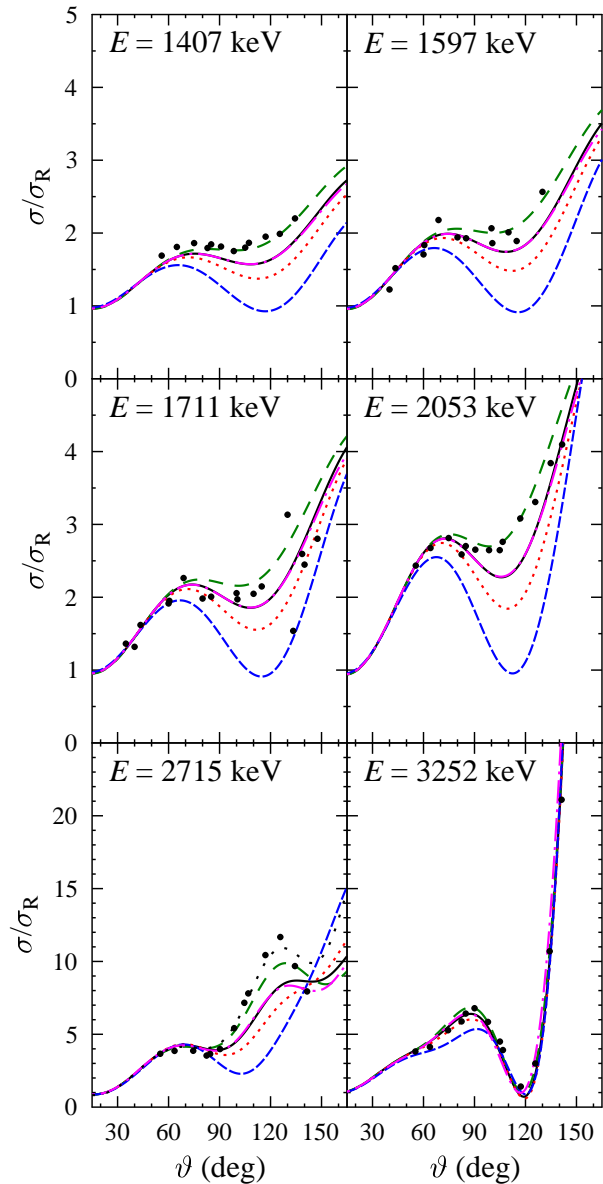


FIG. 5: (Color online) Angular distributions of ${}^3\text{He}(\alpha, \alpha){}^3\text{He}$ elastic scattering, normalized to Rutherford scattering. Experimental data are taken from [31, 44]. The linestyle and color coding is identical to Fig. 4; the dotted black line at $E = 2715$ keV shows the artificial enhancement of the contribution of the $7/2^-$ resonance (see text).

calculated width is $\Gamma_{\text{calc}} = 145$ keV which has to be compared to the experimental width of $\Gamma_{\text{exp}} = 175 \pm 7$ keV (see also Table I). A much better agreement is obtained if the resonance contribution is artificially enhanced in the calculation by an increase of the phase shift of the $7/2^-$ partial wave by about 5° from 10° in the standard calculation to 15° (dotted black line in Fig. 5). The deviation is clearly not related to the potential strength of the even partial waves which will be most important for the analysis of the ${}^3\text{He}(\alpha, \gamma){}^7\text{Be}$ capture cross section in

the next Sec. IV B.

Summarizing the above, an excellent agreement between all experimental scattering data (phase shifts and angular distributions) and the calculated values is obtained using the above derived potential strength parameters $\lambda^{\text{even}} = 1.452$, $\lambda_{LS}^{\text{even}} = 0$, $\lambda^{\text{odd}} = 1.830$ and $\lambda_{LS}^{\text{odd}} = -0.173$ (standard case). The results of all scattering experiments are consistent with each other and can be well described using the present model.

The scattering wave functions can now be calculated without further adjustment of parameters. Because of the dominating external capture (see Fig. 3), good agreement between the predicted and experimental capture cross sections has to be expected. This will be further analyzed in the next Sec. IV B.

B. The ${}^3\text{He}(\alpha, \gamma){}^7\text{Be}$ capture cross section

In addition to the scattering wave function $\chi(r)$, the determination of the DC cross section in Eqs. (2.1) and (2.2) requires the calculation of the bound state wave function $u(r)$. Because of the contributions from the nuclear exterior (see Fig. 3), it is essential that the calculated bound state wave function has the correct asymptotic behavior that is defined by the binding energy. This leads to a slight readjustment of the potential strength parameter λ for the bound states compared to the above results for the scattering phase shifts. The results are $\lambda(3/2^-) = 1.836$ for the ground state of ${}^7\text{Be}$ at $E = -1587$ keV and $\lambda(1/2^-) = 1.799$ for the first excited state of ${}^7\text{Be}$ at $E = -1158$ keV ($E^* = 429$ keV). No spin-orbit potential has been used here.

The remaining calculation of the DC cross section is straightforward and does not require any adjustment to experimental capture data. The results are shown in Fig. 6 with a comparison to the available experimental data and in Fig. 7 in a broader energy range. The calculations take into account all possible $E1$, $E2$, and $M1$ contributions from the incoming scattering waves with $L = 0 - 3$. However, as has been shown in several previous studies, the $E1$ contribution is dominating at all energies. Only in the $7/2^-$ and $5/2^-$ resonances a noticeable $E2$ contribution is found, and the $M1$ contribution remains negligible over the whole energy range. A decomposition into the various contributions has already been shown in Fig. 5 of [22], Fig. 8 of [23], Fig. 8 of [24], Fig. 2 of [26], Fig. 7 of [31], Fig. 2 of [32], Fig. 8 of [35], and Fig. 5 of [38], and is thus not repeated here.

The standard calculation (using the potential strength parameters from the adjustment to the experimental phase shifts) shows an excellent agreement with the total S-factor and the branching ratio $R = \sigma_{429}/\sigma_0$ in the low-energy region below 1 MeV. At higher energies the calculation agrees with the old data of Parker and Kavanagh [4], but is significantly lower than the recent experimental data of [2].

The sensitivity of the ${}^3\text{He}(\alpha, \gamma){}^7\text{Be}$ capture cross sec-

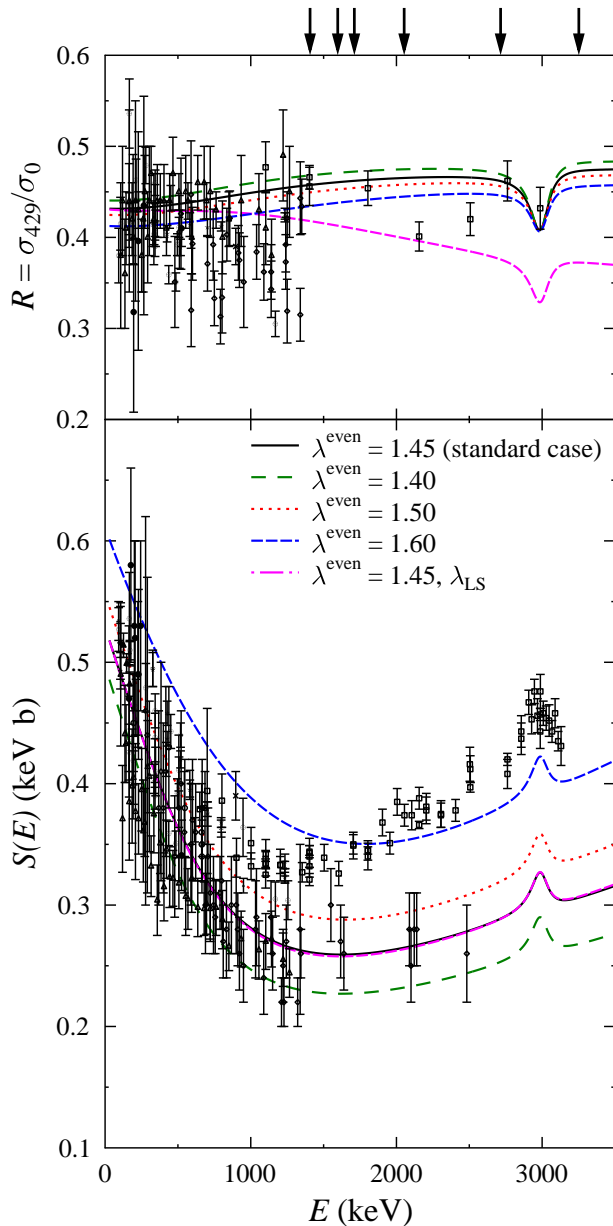


FIG. 6: (Color online) Astrophysical S-factor and branching ratio $R = \sigma_{429}/\sigma_0$ for the ${}^3\text{He}(\alpha,\gamma){}^7\text{Be}$ capture reaction. Experimental data are taken from [2, 3, 4, 5, 6, 7, 8, 9, 10, 11, 12, 13, 14, 15, 16, 17]. The linestyles and color codes are the same as in Figs. 4 and 5. The vertical arrows on top indicate the energies of the angular distributions in the previous Fig. 5 where the elastic scattering cross sections are well reproduced. These scattering data cover the energy range of the recent ${}^3\text{He}(\alpha,\gamma){}^7\text{Be}$ capture data [2] (shown as open squares).

tion on the underlying potential has been studied in the same way as in the previous Sec. IV A by a variation of the λ and λ_{LS} potential strength parameters. The results are also shown in Figs. 6 and 7. In general, an increasing potential strength leads to an increasing S-factor. A

detailed discussion will be given in Sec. V.

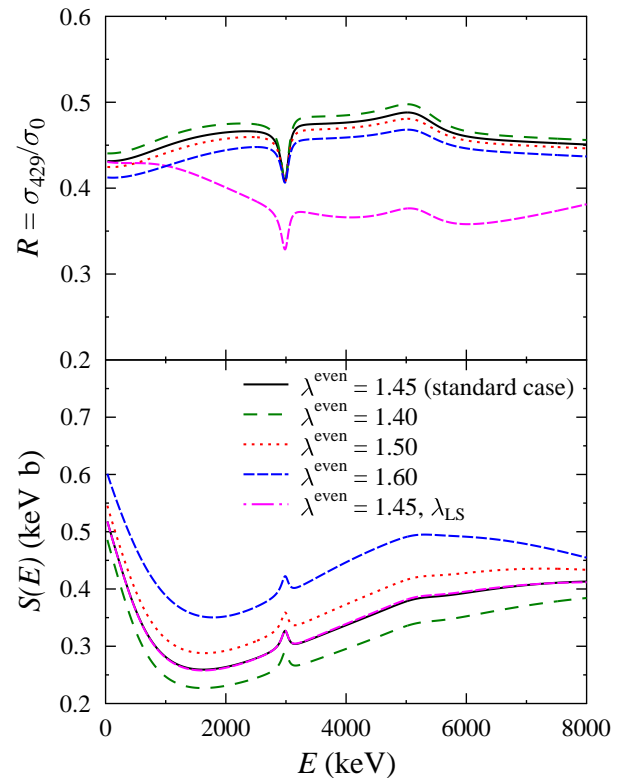


FIG. 7: (Color online) Same as Fig. 6, but with an extended energy range up to 8 MeV. For better visibility of the calculated curves, the experimental data have been omitted. The linestyles and color codes are the same as in the previous Figs. 4, 5, and 6.

Before entering the detailed discussion of the shown ${}^3\text{He}(\alpha,\gamma){}^7\text{Be}$ capture cross sections, the presented results are completed by an analysis of the two $L = 3$ resonances and a study of the low-energy behavior of the astrophysical S-factor. For both resonances it is obvious that the total width Γ is practically identical to the alpha particle width Γ_α . As already shown in Table I, the calculated widths Γ_{calc} agree reasonably well with the experimental results Γ_{exp} . This is also obvious from correct description of the resonant behavior of the $L = 3$ elastic phase shifts in Fig. 4.

The $7/2^-$ resonance at 2983 keV decays by an $E2$ transition to the $3/2^-$ ground state of ${}^7\text{Be}$ whereas no $E2$ transition to the first excited $1/2^-$ state is possible. A Breit-Wigner fit to the calculated capture cross section in this resonance leads to a radiation width $\Gamma_\gamma = \Gamma_{\gamma,0} = 37\text{ meV}$ and a resonance strength $\omega\gamma = 150\text{ meV}$. This prediction is in reasonable agreement with the experimental result of $\omega\gamma = 330 \pm 210\text{ meV}$ [2].

The $5/2^-$ resonance at 5143 keV was not measured yet in the ${}^3\text{He}(\alpha,\gamma){}^7\text{Be}$ reaction. The DC model predicts $\Gamma_{\gamma,0} \approx 50\text{ meV}$ for the $E2$ transition to the $3/2^-$ ground state and $\Gamma_{\gamma,429} \approx 185\text{ meV}$ for the $E2$ tran-

sition to the first excited $1/2^-$ state. This leads to $\Gamma_\gamma = \Gamma_{\gamma,0} + \Gamma_{\gamma,429} \approx 235 \text{ meV}$ or a total resonance strength $\omega\gamma \approx 0.7 \text{ eV}$. Because of the huge width of this resonance, any determination of resonance parameters has relatively large uncertainties. An additional theoretical uncertainty is related to the opening of the ${}^6\text{Li-}p$ channel slightly above 4 MeV .

It is interesting to note that the different decay patterns of the $7/2^-$ and $5/2^-$ resonances are clearly visible in the branching ratio R although the $E2$ contribution to the total cross section is small compared to the dominating $E1$ transitions. Fig. 7 clearly shows a smaller branching ratio in the $7/2^-$ resonance around 3 MeV which can only decay to the $3/2^-$ ground state, and a larger branching ratio in the $5/2^-$ resonance around 5 MeV which predominantly decays to the $1/2^-$ first excited state.

The S-factor at very low energies is extrapolated down to $S(0)$ using the following procedure. The calculated cross sections are fitted using a second-order polynomial up to 500 keV . The results for $S(0)$ and $S'(0)/S(0)$ are listed in Table II for the different potentials shown in Figs. 4, 5, 6, and 7. The standard case leads to $S(0) = 0.53 \text{ keV b}$ and $S'(0)/S(0) = -0.73 \text{ MeV}^{-1}$, in agreement with the compilation of solar fusion cross sections by Adelberger *et al.* [18] who recommend $S(0) = 0.53 \pm 0.05 \text{ keV b}$ and $S'(0)/S(0) = -0.57 \text{ MeV}^{-1}$, and the NACRE compilation [19] where $S(0) = 0.54 \pm 0.09 \text{ keV b}$ and $S'(0)/S(0) = -0.96 \text{ MeV}^{-1}$ are given. The recent summary of Cyburt and Davids [40] recommends a slightly higher value of $S(0) = 0.580 \pm 0.043 \text{ keV b}$ and $S'(0)/S(0) = -0.92 \pm 0.18 \text{ MeV}^{-1}$. Variations of the order of about 10% for the slope of the S-factor at zero energy are found using the different potentials. Such variations are also typical for the different theoretical calculations in [20, 21, 22, 23, 24, 25, 26, 27, 28, 29, 30, 31, 32, 33, 34, 35, 36, 37, 38, 39]. The adopted $S'(0)/S(0)$ [18, 19, 40] show somewhat larger variations. The average of the three compilations of $S'(0)/S(0) = -0.82 \text{ MeV}^{-1}$ is in reasonable agreement with the calculated $S'(0)/S(0) = -0.73 \text{ MeV}^{-1}$ in the standard case and in perfect agreement with the calculation using $\lambda^{\text{even}} = 1.40$ where $S'(0)/S(0) = -0.79 \text{ MeV}^{-1}$ is found. However, larger values $\lambda^{\text{even}} > 1.50$ correspond to lower $S'(0)/S(0)$.

Using the standard case potential, $S(0) = 0.53 \text{ keV b}$ is predicted from the present study. This prediction depends on the theoretical spectroscopic factors C^2S of the bound state wave functions. From the excellent agreement between the experimental and calculated capture cross sections and branching ratios at low energies (see Fig. 6) it is obvious that the chosen theoretical spectroscopic factors [49] are correct within about 10%. Any minor readjustment of these spectroscopic factors will affect the the calculated capture cross sections linearly at all energies, but will not affect the calculated energy dependence of the ${}^3\text{He}(\alpha,\gamma){}^7\text{Be}$ capture cross section. Also the normalized slope $S'(0)/S(0)$ will not be affected by a readjustment of the spectroscopic factors.

TABLE II: Extrapolated astrophysical S-factor $S(0)$ at zero energy and its normalized derivative $S'(0)/S(0)$ for different potentials. The strength parameters $\lambda^{\text{odd}} = 1.830$ and $\lambda_{LS}^{\text{odd}} = -0.173$ have not been varied. For comparison, the results of recent compilations [18, 19, 40] are also listed.

λ^{even}	$\lambda_{LS}^{\text{even}}$	$S(0)$ (keV b)	$S'(0)/S(0)$ (MeV^{-1})	remarks
1.45	0.0	0.530	-0.731	standard case
1.40	0.0	0.497	-0.791	
1.50	0.0	0.557	-0.666	
1.60	0.0	0.611	-0.536	
1.45	-0.173	0.530	-0.733	close to Ref. [31]
-	-	0.53 ± 0.05	-0.57	Adelberger <i>et al.</i> [18]
-	-	0.54 ± 0.09	-0.96	NACRE [19]
-	-	0.580 ± 0.043	-0.92	Cyburt and Davids [40]

The chosen DC model does not require effective charges and uses $q = +2e$ for the involved ${}^3\text{He}$ and ${}^4\text{He}$ nuclei. An additional introduction of effective charges in the model may affect the absolute values of the DC cross sections. Because of the dominating $E1$ contribution to the capture cross section, the introduction of effective charges does not affect the calculated energy dependence in a significant way. Similar to the statements on the spectroscopic factor in the previous paragraph, effective charges do also not affect the normalized slope $S'(0)/S(0)$ of the astrophysical S-factor. Although effective charges cannot be determined from scattering phase shifts, it is obvious from the excellent agreement between the experimental and calculated cross sections at low energies that the effective charges cannot deviate strongly from the used real charges.

V. DISCUSSION AND CONCLUSIONS

It has been shown in the previous Sects. IV A and IV B that the standard calculation with the parameters $\lambda^{\text{even}} = 1.45$, $\lambda_{LS}^{\text{even}} = 0$, $\lambda^{\text{odd}} = 1.83$, and $\lambda_{LS}^{\text{odd}} = -0.173$ is able to describe elastic scattering phase shifts for ${}^3\text{He}(\alpha,\alpha){}^3\text{He}$ reaction in the full energy range up to about 8 MeV and the ${}^3\text{He}(\alpha,\gamma){}^7\text{Be}$ capture cross sections to the ${}^7\text{Be}$ ground state and first excited state at low energies. At higher energies the calculation agrees with the old data [4] but disagrees with the new data [2]. In the following discussion the theoretical uncertainties will be analyzed, and the question will be answered whether the new data of [2] can be described within the present model. Most of the considerations will also be valid for other models because of the dominating external contributions to the ${}^3\text{He}(\alpha,\gamma){}^7\text{Be}$ capture cross section. The discussion will focus on the dominating $E1$ contributions from the incoming s -wave and d -wave.

The analysis of elastic scattering clearly shows that the s -wave and d -wave phase shifts can only be reproduced

using the potential strength of the standard calculation (see Figs. 4 and 5). For the s -wave $\lambda^{\text{even}} = 1.40 - 1.45$ is the acceptable range. The d -wave phase shifts which remain close to zero up to about 8 MeV can only be described with λ values very close to $\lambda^{\text{even}} = 1.45$. A value of $\lambda^{\text{even}} > 1.50$ can clearly be excluded. This is further strengthened by the analysis of the slope $S'(0)/S(0)$ at low energies, see Table II.

The integrand of the DC integral in Eq. (2.2), i.e. the overlap between scattering wave function $\chi(r)$, electromagnetic operator \mathcal{O}^{E1} , and bound state wave function $u(r)$, is shown for the standard calculation in Fig. 3. The upper part shows the $E1$ transition from the s -wave to the ground state and first excited state, and the middle part shows the $E1$ transition from the d -wave to the ground state in ${}^7\text{Be}$. As usual, the integrand is shifted towards the exterior for lower energies. But it has to be pointed out that all curves are clearly dominated by contributions from far outside the nucleus at both considered energies $E = 100\text{ keV}$ and 3 MeV ; i.e., also at the high energy $E = 3\text{ MeV}$ the external contribution dominates. Thus, the result of the DC calculation is essentially defined by the behavior of the scattering wave function $\chi(r)$ and the bound state wave function $u(r)$ at radii between 5 fm and 35 fm that is much larger than the size of ${}^7\text{Be}$. Any calculation with realistic nuclear potentials should provide a more or less similar capture cross section if the potential is able to reproduce the elastic phase shifts. This is particularly true for the calculated energy dependence.

The absolute value of the bound state wave function $u(r)$ in the external region depends indirectly on the chosen potential shape. The slope of the external part of the bound state wave function $u(r)$ is well defined by the binding energy, but the normalization of the bound state wave function $u(r)$

$$\int_0^\infty u^2(r) dr = 1 \quad (5.1)$$

has its main contribution from smaller radii $r < 5\text{ fm}$, i.e. from the nuclear interior and surface (see Fig. 2). In line with the considerations in [50], the chosen spectroscopic factors $C^2S \approx 1.2$ for the ground state and first excited state in ${}^7\text{Be}$ simply mean here that the bound state wave functions $u(r)$ in the nuclear exterior have to be scaled by a factor $\sqrt{C^2S} \approx 1.1$ to bring the calculated DC cross section into agreement with the experimental data at low energies. The choice of a different potential leads to a different shape of the wave function $u(r)$ and its asymptotic behavior that can be compensated by a different spectroscopic factor. Finally, the theoretical cross section, in particular its energy dependence, will remain almost unaffected – provided that the phase shifts are well reproduced.

Nevertheless, an attempt has been made to reproduce the new ${}^3\text{He}(\alpha,\gamma){}^7\text{Be}$ capture data [2] within the present model. In general, an increasing nuclear potential strength decreases the Coulomb barrier and thus in-

creases the calculated capture cross section. A value of $\lambda^{\text{even}} \approx 1.6$ is required to reproduce the larger cross section data of [2]. The calculated capture cross section at low energies is increased by about 15% compared to the standard case which is slightly higher than the allowed range of the precision experiments at low energies. This larger potential strength also leads to a strong disagreement with the scattering data. In particular, the elastic scattering angular distributions in Fig. 5 cannot be described with the increased value of $\lambda^{\text{even}} = 1.6$. These angular distributions have been measured in an energy range that covers the energy range of the recent ${}^3\text{He}(\alpha,\gamma){}^7\text{Be}$ capture data [2] (indicated by the arrows on top of Fig. 6). Taking into account the above considerations on the radial behavior of the overlap integral in Eq. (2.2), it can be excluded that the DC model is able to reproduce simultaneously ${}^3\text{He}(\alpha,\alpha){}^3\text{He}$ elastic scattering [31, 41, 42, 43, 44] and ${}^3\text{He}(\alpha,\gamma){}^7\text{Be}$ capture [2] at energies around 2 – 3 MeV.

It is interesting to note that the branching ratio $R = \sigma_{429}/\sigma_0$ is practically not affected by the variation of the potential strength of the s - and d -waves because both transitions are increased in the same way when λ^{even} is increased from its standard value of 1.45 to about 1.6 to fit the higher capture data of [2]. However, the branching ratio R is significantly affected by the spin-orbit potential of the d -wave. Using the spin-orbit potential strength from the odd partial waves also for the even partial waves ($\lambda_{LS}^{\text{even}} = -0.173$ instead of the standard case $\lambda_{LS}^{\text{even}} = 0$), the effective strength of the potential for the $d_{5/2}$ ($d_{3/2}$) wave is increased (decreased). As pointed out above, an increased potential strength leads to increased capture cross sections. Because there is only an $E1$ transition from the $d_{5/2}$ wave to the $3/2^-$ ground state, but no $E1$ transition to the $1/2^-$ first excited state, the ground state contribution is enhanced, and thus the branching ratio R decreases at higher energies (see Figs. 6 and 7). However, at low energies the dominating contribution to the capture cross section comes from the s -wave which is not affected by the spin-orbit potential, and the branching ratio R at very low energies is practically identical to the standard case.

It is difficult to find an explanation for the discrepancy between the calculated ${}^3\text{He}(\alpha,\gamma){}^7\text{Be}$ capture cross sections and the recent experimental data [2]. Experimental scattering data have been obtained in a series of independent experiments [31, 41, 42, 43, 44, 45, 46] that agree well with each other. The determination of the scattering wave function in the DC integral in Eq. (2.2) is thus very well-defined. Although the requested accuracy of a few per cent for astrophysical modelling has not yet been achieved for the ${}^3\text{He}(\alpha,\gamma){}^7\text{Be}$ capture reaction, all experimental capture data at low energies agree within each other at a 10 – 15% level. The spectroscopic factors – taken as normalization factors in Eq. (2.2) – are thus also well-defined at this level. The same level of accuracy should then be expected for the energy range of the new ${}^3\text{He}(\alpha,\gamma){}^7\text{Be}$ capture data [2] up to about

3 MeV. Instead, the standard calculation underestimates the new capture data by about 30 – 40 %. It has to be pointed out that a wrong normalization of the new data [2] is also very unlikely because the experiment has studied the ${}^3\text{He}(\alpha,\gamma){}^7\text{Be}$ capture reaction very carefully using three different independent techniques (recoil detection, γ detection, and activation) that agree very well with each other at the level of a few per cent. Of course, an independent confirmation of the new data in [2] is nevertheless highly desirable, in particular, because of the discrepancy between the old data in [4] and the new data in [2].

The only remaining explanation is that the DC model itself is not appropriate for the description of the ${}^3\text{He}(\alpha,\gamma){}^7\text{Be}$ capture reaction. However, even “exotic” theoretical solutions like other electromagnetic transitions (except $E1$, $E2$, and $M1$) or further unobserved bound states in ${}^7\text{Be}$ can be excluded at the requested level of 30 – 40 % from the agreement of the different experimental techniques in [2]. And because of the dominating external contributions to the DC cross section, any theoretical calculation that reproduces the scattering phase shifts, should provide a similar theoretical energy dependence and thus underestimate the new capture data for the ${}^3\text{He}(\alpha,\gamma){}^7\text{Be}$ reaction in [2] in a similar way.

VI. SUMMARY

The ${}^3\text{He}(\alpha,\alpha){}^3\text{He}$ elastic scattering and ${}^3\text{He}(\alpha,\gamma){}^7\text{Be}$ capture cross sections have been studied within the DC

model together with folding potentials. It is shown that the elastic scattering phase shifts are well reproduced over a broad energy range. Whereas the low-energy capture data are well described simultaneously with the phase shifts, there is a significant underestimation of the recent capture data [2], but agreement with the old data of [4]. As the DC calculation is very well constrained by experimental scattering data over the whole energy range studied in [2], it is difficult to find an explanation for the discrepancy between the calculated and the recently measured capture cross section of the ${}^3\text{He}(\alpha,\gamma){}^7\text{Be}$ reaction. Further experimental and theoretical effort is needed to resolve this surprising problem.

Acknowledgments

Encouraging discussions and all the support in reconstructing old experimental data is gratefully acknowledged - many thanks to A. Barnard, R. Cyburt, B. Davids, P. Descouvemont, T. Hehl, and F. Strieder.

-
- [1] R. H. Cyburt, B. D. Fields, K. A. Olive, *Phys. Rev. D* **69**, 123519 (2004).
- [2] A. Di Leva, L. Gialanella, R. Kunz, D. Rogalla, D. Schürmann, F. Strieder, M. De Cesare, N. De Cesare, A. D’Onofrio, Zs. Fülöp, Gy. Gyürky, G. Imbriani, G. Mangano, A. Ordine, V. Roca, C. Rolfs, M. Romano, E. Somorjai, F. Terrasi, *Phys. Rev. Lett.*, submitted.
- [3] H. D. Holmgren and R. L. Johnston, *Phys. Rev.* **113**, 1556 (1959).
- [4] P. Parker and R. Kavanagh, *Phys. Rev.* **131**, 2578 (1963).
- [5] K. Nagatani, M. R. Dwarakanath, D. Ashery, *Nucl. Phys.* **A128**, 325 (1969).
- [6] H. Kräwinkel, H. W. Becker, L. Buchmann, J. Görres, K. U. Kettner, W. E. Kieser, R. Santo, P. Schmalbrock, H. P. Trautvetter, A. Vlieks, C. Rolfs, J. W. Hammer, R. E. Azuma, W. S. Rodney, *Z. Phys. A* **304**, 307 (1982).
- [7] R. G. H. Robertson, P. Dyer, T. J. Bowles, R. E. Brown, N. Jarmie, C. J. Maggiore, S. M. Austin, *Phys. Rev. C* **27**, 11 (1983).
- [8] H. Volk, H. Kräwinkel, R. Santo, L. Wallek, *Z. Phys. A* **310**, 91 (1983).
- [9] T. K. Alexander, G. C. Ball, W. N. Lennard, H. Geissel, H.-B. Mak, *Nucl. Phys.* **A427**, 526 (1984).
- [10] J. L. Osborne, C. A. Barnes, R. W. Kavanagh, R. M. Kremer, G. J. Mathews, J. L. Zyskind, P. D. Parker, A. J. Howard, *Phys. Rev. Lett.* **48**, 1664 (1982); *Nucl. Phys.* **A419**, 115 (1984).
- [11] M. Hilgemeier, H. W. Becker, C. Rolfs, H. P. Trautvetter, J. W. Hammer, *Z. Phys. A* **329**, 243 (1988).
- [12] B. S. Nara Singh, M. Hass, Y. Nir-El, G. Haquin, *Phys. Rev. Lett.* **93**, 262503 (2004).
- [13] D. Bemmerer, F. Confortola, H. Costantini, A. Formicola, Gy. Gyürky, R. Bonetti, C. Broggin, P. Corvisiero, Zs. Elekes, Zs. Fülöp, G. Gervino, A. Guglielmetti, C. Gustavino, G. Imbriani, M. Junker, M. Laubenstein, A. Lemut, B. Limata, V. Lozza, M. Marta, R. Menegazzo, P. Prati, V. Roca, C. Rolfs, C. Rossi Alvarez, E. Somorjai, O. Straniero, F. Strieder, F. Terrasi, H. P. Trautvetter, *Phys. Rev. Lett.* **97**, 122502 (2006).
- [14] Gy. Gyürky, F. Confortola, H. Costantini, A. Formicola, D. Bemmerer, R. Bonetti, C. Broggin, P. Corvisiero, Zs. Elekes, Zs. Fülöp, G. Gervino, A. Guglielmetti, C. Gustavino, G. Imbriani, M. Junker, M. Laubenstein, A. Lemut, B. Limata, V. Lozza, M. Marta, R. Menegazzo, P. Prati, V. Roca, C. Rolfs, C. Rossi Alvarez, E. Somorjai, O. Straniero, F. Strieder, F. Terrasi, H. P. Trautvetter, *Phys. Rev. C* **75**, 035805 (2007).
- [15] F. Confortola, D. Bemmerer, H. Costantini, A. Formicola, Gy. Gyürky, P. Bezzon, R. Bonetti, C. Broggin, P. Corvisiero, Zs. Elekes, Zs. Fülöp, G. Gervino, A. Gugliel-

- metti, C. Gustavino, G. Imbriani, M. Junker, M. Laubenstein, A. Lemut, B. Limata, V. Lozza, M. Marta, R. Menegazzo, P. Prati, V. Roca, C. Rolfs, C. Rossi Alvarez, E. Somorjai, O. Straniero, F. Strieder, F. Terrasi, H. P. Trautvetter, Phys. Rev. C **75**, 065803 (2007).
- [16] T. A. D. Brown, C. Bordeanu, K. A. Snover, D. W. Storm, D. Melconian, A. L. Sallaska, S. K. L. Sjue, S. Triambak, Phys. Rev. C **76**, 055801 (2007).
- [17] H. Costantini, D. Bemmerer, F. Confortola, A. Formicola, Gy. Gyürky, P. Bezzon, R. Bonetti, C. Brogginì, P. Corvisiero, Zs. Elekes, Zs. Fülöp, G. Gervino, A. Guglielmetti, C. Gustavino, G. Imbriani, M. Junker, M. Laubenstein, A. Lemut, B. Limata, V. Lozza, M. Marta, R. Menegazzo, P. Prati, V. Roca, C. Rolfs, C. Rossi Alvarez, E. Somorjai, O. Straniero, F. Strieder, F. Terrasi, H. P. Trautvetter, Nucl. Phys. **A814**, 144 (2008).
- [18] E. G. Adelberger, S. M. Austin, J. N. Bahcall, A. B. Balantekin, G. Bogaert, L. S. Brown, L. Buchmann, F. E. Cecil, A. E. Champagne, L. de Braekeleer, C. A. Duba, S. R. Elliott, S. J. Freedman, M. Gai, G. Goldring, C. R. Gould, A. Gruzinov, W. C. Haxton, K. M. Heeger, E. Henley, C. W. Johnson, M. Kamionkowski, R. W. Kavanagh, S. E. Koonin, K. Kubodera, K. Langanke, T. Motobayashi, V. Pandharipande, P. Parker, R. G. H. Robertson, C. Rolfs, R. F. Sawyer, N. Shaviv, T. D. Shoppa, K. A. Snover, E. Swanson, R. E. Tribble, S. Turck-Chieze, J. F. Wilkerson, Rev. Mod. Phys. **70**, 1265 (1998).
- [19] C. Angulo, M. Arnould, M. Rayet, P. Descouvemont, D. Baye, C. Leclercq-Willain, A. Coc, S. Barhoumi, P. Aguer, C. Rolfs, R. Kunz, J. W. Hammer, A. Mayer, T. Paradellis, S. Kossionides, C. Chronidou, K. Spyrou, S. Degl'Innocenti, G. Fiorentini, B. Ricci, S. Zavatarelli, C. Providencia, H. Wolters, J. Soares, C. Grama, J. Rahighi, A. Shotter, M. Laméhi Rachti, Nucl. Phys. **A656**, 3 (1999).
- [20] R. F. Christy and I. Duck, Nucl. Phys. **24**, 89 (1961).
- [21] T. A. Tombrello and G. C. Phillips, Phys. Rev. **122**, 224 (1961).
- [22] T. A. Tombrello and P. D. Parker, Phys. Rev. **131**, 2582 (1963).
- [23] B. T. Kim, T. Izumoto, K. Nagatani, Phys. Rev. C **23**, 33 (1981).
- [24] Q. K. K. Liu, H. Kanada, Y. C. Tang, Phys. Rev. C **23**, 645 (1981).
- [25] H. Walliser, Q. K. K. Liu, H. Kanada, Y. C. Tang, Phys. Rev. C **28**, 57 (1983).
- [26] T. Mertelmeier and H. M. Hofmann, Nucl. Phys. **A459**, 387 (1986).
- [27] T. Kajino and A. Arima, Phys. Rev. Lett. **52**, 739 (1984).
- [28] H. Walliser, H. Kanada, Y. C. Tang, Phys. Rev. Lett. **53**, 399 (1984).
- [29] T. Kajino, H. Toki, S. M. Austin, Astrophys. J. **319**, 531 (1987).
- [30] B. Buck and A. C. Merchant, J. Phys. G **14**, L211 (1988).
- [31] P. Mohr, H. Abele, R. Zwiebel, G. Staudt, H. Krauss, H. Oberhammer, A. Denker, J. W. Hammer, G. Wolf, Phys. Rev. C **48** 1420 (1993).
- [32] S. B. Dubovichenko and A. V. Dzhezairov-Kakhramanov, Phys. Atom. Nucl. **58**, 579 (1995); Yad. Fiz. **58**, 635 (1995); *nucl-th/9802080*.
- [33] D. Baye and E. Brainis, Phys. Rev. C **61**, 025801 (2000).
- [34] A. Csótó and K. Langanke, Few Body Systems **29**, 121 (2000).
- [35] K. Nollelt, Phys. Rev. C **63**, 054002 (2001).
- [36] P. Descouvemont, A. Adahchour, C. Angulo, A. Coc, E. Vangioni-Flam, At. Data Nucl. Data Tables **88**, 203 (2004).
- [37] L. Canton and L. G. Levchuk, Nucl. Phys. **A808**, 192 (2008).
- [38] A. Mason, R. Chatterjee, L. Fortunato, A. Vitturi, Europ. Phys. J. A **39**, 107 (2009).
- [39] P. Navratil, S. Quaglioni, I. Stetcu, B. R. Barrett, J. Phys. G **36**, 083101 (2009).
- [40] R. H. Cyburt and B. Davids, Phys. Rev. C **78**, 064614 (2008).
- [41] R. Spiger and T. A. Tombrello, Phys. Rev. **163**, 964 (1967).
- [42] W. R. Boykin, S. D. Baker, D. M. Hardy, Nucl. Phys. **A195**, 241 (1972).
- [43] D. M. Hardy, R. J. Spiger, S. D. Baker, Y. S. Chen, T. A. Tombrello, Nucl. Phys. **195**, 250 (1972).
- [44] A. C. L. Barnard, C. M. Jones, G. C. Phillips, Nucl. Phys. **50**, 629 (1964).
- [45] M. Ivanovich, P. G. Young, G. G. Ohlsen, Nucl. Phys. **A110**, 441 (1968).
- [46] L. S. Chuang, Nucl. Phys. **A174**, 399 (1971).
- [47] D. R. Tilley, C. M. Cheves, J. L. Godwin, G. M. Hale, H. M. Hofmann, J. H. Kelley, C. G. Sheu, H. R. Weller, Nucl. Phys. **A708**, 3 (2002).
- [48] K. H. Kim, M. H. Park, B. T. Kim, Phys. Rev. C **35**, 363 (1987).
- [49] D. Kurath and D. J. Millener, Nucl. Phys. **A238**, 269 (1975).
- [50] C. Iliadis, C. Angulo, P. Descouvemont, M. Lugaro, P. Mohr, Phys. Rev. C **77**, 045802 (2008).
- [51] A. M. Mukhamedzhanov, F. M. Nunes, P. Mohr, Phys. Rev. C **77**, 051601(R) (2008).
- [52] G. R. Satchler and W. G. Love, Phys. Rep. **55**, 183 (1979).
- [53] A. M. Kobos, B. A. Brown, R. Lindsay, and R. Satchler, Nucl. Phys. **A425**, 205 (1984).
- [54] H. de Vries, C. W. de Jager, and C. de Vries, At. Data Nucl. Data Tables **36**, 495 (1987).
- [55] H. Walliser and T. Fliessbach, Phys. Rev. C **31**, 2242 (1985).
- [56] B. Buck, R. A. Baldock, J. Alberto-Rubio, J. Phys. G **11**, L11 (1985).
- [57] J. H. Kelley, D. R. Tilley, H. R. Weller, H. H. Hasan, Nucl. Phys. **A474**, 1 (1987).
- [58] P. Mohr, V. Kölle, S. Wilmes, U. Atzrott, G. Staudt, J. W. Hammer, H. Krauss, H. Oberhammer, Phys. Rev. C **50**, 1543 (1994).